Is PET Radiomics Useful to Predict Pathologic Tumor Response and Prognosis in Locally Advanced Cervical Cancer?

Angela Collarino*[1], Vanessa Feudo*[2], Tina Pasciuto[3], Anita Florit[2], Elisabeth Pfaehler[4], Marco de Summa[5], Nicolò Bizzarri[6], Salvatore Annunziata[1], Gian Franco Zannoni[7,8], Lioe-Fee de Geus-Oei[9–11], Gabriella Ferrandina[6,12], Maria Antonietta Gambacorta[13,14], Giovanni Scambia[6,12], Ronald Boellaard[15], Evis Sala[14,16], Vittoria Rufini[1,2], and Floris HP van Velden[9]

[1]Nuclear Medicine Unit, Fondazione Policlinico Universitario A. Gemelli–IRCCS, Rome, Italy; [2]Section of Nuclear Medicine, University Department of Radiological Sciences and Hematology, Università Cattolica del Sacro Cuore, Rome, Italy; [3]Research Core Facility Data Collection G-STeP, Fondazione Policlinico Universitario A. Gemelli–IRCCS, Rome, Italy; [4]Institute of Neuroscience and Medicine, INM-4, Forschungszentrum Jülich GmbH, Jülich, Germany; [5]PET/CT Center, Fondazione Policlinico Universitario A. Gemelli-IRCCS, Rome, Italy; [6]Gynecologic Oncology Unit, Department of Woman and Child Health and Public Health, Fondazione Policlinico Universitario A. Gemelli–IRCCS, Rome, Italy; [7]Gynecopathology Unit, Department of Woman and Child Health and Public Health, Fondazione Policlinico Universitario A. Gemelli–IRCCS, Rome, Italy; [8]Section of Pathology, Department of Woman and Child Health and Public Health, Università Cattolica del Sacro Cuore, Rome, Italy; [9]Section of Nuclear Medicine, Department of Radiology, Leiden University Medical Center, Leiden, The Netherlands; [10]Biomedical Photonic Imaging Group, MIRA Institute, University of Twente, Enschede, The Netherlands; [11]Department of Radiation Science and Technology, Technical University of Delft, Delft, The Netherlands; [12]Section of Obstetrics and Gynecology, University Department of Life Sciences and Public Health, Università Cattolica del Sacro Cuore, Roma, Italy; [13]Radiation Oncology Unit, Fondazione Policlinico Universitario A. Gemelli–IRCCS, Roma, Italy; [14]Section of Radiology, University Department of Radiological Sciences and Hematology, Università Cattolica del Sacro Cuore, Rome, Italy; [15]Department of Radiology and Nuclear Medicine, Amsterdam UMC, Location VU University Medical Center, Amsterdam, The Netherlands; and [16]Advanced Radiodiagnostics Centre, Fondazione Policlinico Universitario A. Gemelli–IRCCS, Rome, Italy

This study investigated whether radiomic features extracted from pretreatment [18F]FDG PET could improve the prediction of both histopathologic tumor response and survival in patients with locally advanced cervical cancer (LACC) treated with neoadjuvant chemoradiotherapy followed by surgery compared with conventional PET parameters and histopathologic features. **Methods:** The medical records of all consecutive patients with LACC referred between July 2010 and July 2016 were reviewed. [18F]FDG PET/CT was performed before neoadjuvant chemoradiotherapy. Radiomic features were extracted from the primary tumor volumes delineated semiautomatically on the PET images and reduced by factor analysis. A receiver-operating-characteristic analysis was performed, and conventional and radiomic features were dichotomized with Liu's method according to pathologic response (pR) and cancer-specific death. According to the study protocol, only areas under the curve of more than 0.70 were selected for further analysis, including logistic regression analysis for response prediction and Cox regression analysis for survival prediction. **Results:** A total of 195 patients fulfilled the inclusion criteria. At pathologic evaluation after surgery, 131 patients (67.2%) had no or microscopic (≤3 mm) residual tumor (pR0 or pR1, respectively); 64 patients (32.8%) had macroscopic residual tumor (>3 mm, pR2). With a median follow-up of 76.0 mo (95% CI, 70.7–78.7 mo), 31.3% of patients had recurrence or progression and 20.0% died of the disease. Among conventional PET parameters, SUV$_{mean}$ significantly differed between pathologic responders and nonresponders. Among radiomic features, 1 shape and 3 textural features significantly differed between pathologic responders and nonresponders. Three radiomic features significantly differed between presence and absence of recurrence or progression and between presence and absence of cancer-specific death. Areas under the curve were less than 0.70 for all parameters; thus, univariate and multivariate regression analyses were not performed. **Conclusion:** In a large series of patients with LACC treated with neoadjuvant chemoradiotherapy followed by surgery, PET radiomic features could not predict histopathologic tumor response and survival. It is crucial to further explore the biologic mechanism underlying imaging-derived parameters and plan a large, prospective, multicenter study with standardized protocols for all phases of the process of radiomic analysis to validate radiomics before its use in clinical routine.

Key Words: locally advanced cervical cancer; radiomics; [18F]FDG PET/CT; response to therapy; prognosis

Cervical cancer is one of the most common malignancies in women worldwide (*1*). According to international guidelines (*2,3*), the preferred treatment for patients with locally advanced cervical cancer (LACC) is definitive cisplatin-based chemoradiotherapy followed by brachytherapy. However, the disease recurs in one third of LACC patients, usually within 2 y after chemoradiotherapy, and the 5-y overall survival is around 70% (*4,5*). Neoadjuvant chemoradiotherapy followed by radical surgery is an alternative strategy, aiming to remove residual tumor that is resistant to

chemoradiotherapy. It has been shown that persistence of pathologic residual tumor predicts poor survival in patients treated with this approach (6,7).

Recently, there has been growing interest in the extraction and analysis of a variety of quantitative features from medical images, including [18F]FDG PET/CT, denoted as radiomics (8–10). In essence, radiomics comprises the shape, intensity, and textural features of the tumor. Shape features describe geometric characteristics of tumors and provide morphologic characterization of [18F]FDG uptake within a specified volume of interest (VOI). Intensity features describe the intensity signal variations in the tumor volume, without reference to their spatial distribution. Textural features are extracted from statistical matrices on the basis of local intensity spatial distribution relationships and reflect tumor [18F]FDG distribution and, so, its heterogeneity (11). These features could better predict the histopathologic markers, therapy response, and prognosis than could conventional imaging parameters such as SUV_{max}, SUV_{mean}, SUV_{peak}, metabolically active tumor volume, and total lesion glycolysis (12). Previous studies performed on LACC patients treated with exclusive chemoradiotherapy have investigated the use of radiomics derived from pretreatment PET/CT for predicting response to therapy (13–15) as well as survival (15–25). Even though the results reported are difficult to compare because of the large variability in methodology and lack of standardization, most of the studies showed that texture features were significantly predictive of response (13–15) and that the combination of radiomic and clinical features was significantly predictive of recurrence and survival (16,17,19,21–23). The aim of our study was to investigate whether radiomic features extracted from pretreatment [18F]FDG PET could predict histopathologic tumor response and survival in LACC patients treated with neoadjuvant chemoradiotherapy followed by surgery in comparison with conventional PET parameters and histopathologic features.

MATERIALS AND METHODS

Patients and Study Protocol

This retrospective study was approved by the Ethical Committee of Fondazione Policlinico Universitario A. Gemelli–IRCCS (study code 3860), and all subjects gave written informed consent. The medical records of all consecutive LACC patients who were referred to the Gynecologic Oncology Unit between July 2010 and July 2016 were reviewed. Women were included if they were at least 18 y old, underwent pretreatment [18F]FDG PET/CT, and received neoadjuvant chemoradiotherapy followed by radical surgery. Additionally, a primary tumor of at least 2.6 cm in diameter on MRI (available in all patients) was necessary to allow heterogeneity quantification on PET, which requires spheric volumes to be larger than 10 cm^3 (26). Patients were excluded if they had distant metastatic disease, prior locoregional surgery, prior chemotherapy, locoregional radiation therapy within 5 y, or a plasma glucose level of more than 200 mg/dL before the [18F]FDG PET/CT acquisition.

[18F]FDG PET/CT Image Acquisition

Pretreatment [18F]FDG PET/CT was performed as previously described (27). Briefly, images were acquired at a median of 65 min (range, 52–78 min) after intravenous administration of 2.5–4 MBq of [18F]FDG per kilogram on a Gemini GXL (Philips Healthcare) or Biograph mCT (Siemens Healthineers) PET/CT scanner. A low-dose CT scan (110–120 kV, 20–40 mAs) and PET scan (2.5–3.0 min per bed position) were acquired from skull to pelvis according to the European Association of Nuclear Medicine guidelines (28) and reconstructed in
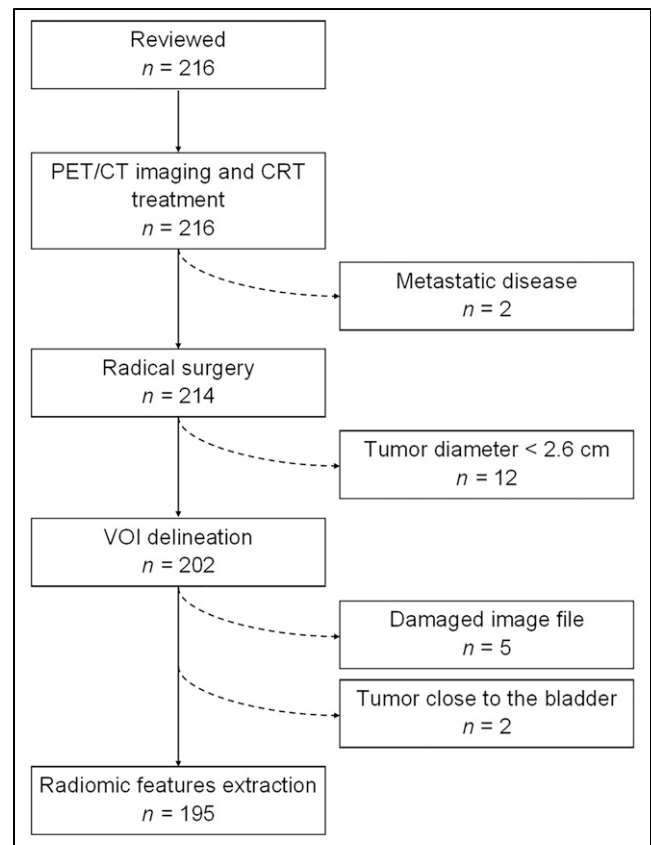

FIGURE 1. Flowchart of study population.

line with the 18F standard 1 provided by the European Association of Nuclear Medicine Research Ltd.

Image Analysis

All PET/CT images were reviewed by consensus between 2 nuclear medicine physicians (with 3 and 8 y of experience), who were masked to clinical, histopathologic, and follow-up information.

VOIs of the primary tumor were drawn semiautomatically with the ACCURATE software (29,30) on all PET images using a background-corrected 50% isocontour of the body-weighted SUV_{peak}, defined as the highest SUV_{mean} of a 1-mL sphere within the VOI (31). Areas of high [18F]FDG uptake close to the primary tumor (e.g., bladder, kidneys, ureters) were excluded manually when necessary. The conventional PET parameters SUV_{max}, SUV_{mean}, SUV_{peak}, metabolically active tumor volume, and total lesion glycolysis were extracted from the original VOIs. In addition, 477 radiomic features were extracted using RaCaT 1.27 software (32). Detailed information about the radiomic features can be found in the supplemental materials (available at http://jnm.snmjournals.org) (11,30,32).

Neoadjuvant Chemoradiotherapy

Neoadjuvant radiotherapy included whole-pelvis irradiation (10.8 cGy/fraction, 22 fractions) with a total dose of 39.6 Gy, and an additional dose of 10.8 Gy to the primary tumor and parametrium through the concomitant boost technique (0.9 cGy/fraction, 12 fractions every other day). Concomitant chemotherapy included cisplatin (20 mg/m^2, 2-h intravenous infusion) during the first 4 d and last 4 d of treatment, and capecitabine (1,300 mg/m^2/daily, orally administered) during the first 2 wk and last 2 wk of treatment (33).

TABLE 1
Clinical, Pathologic, and Treatment Characteristics and Oncologic Outcomes of Whole Study Population ($n = 195$)

| Characteristic	Data
Age at diagnosis (y)	
Mean ± SD	51 ± 12
Median	51 (range, 20–77)
Body mass index (kg/m^2)*	24.0 (range, 15.6–44.5)
Clinical 2009 FIGO stage (n)	
IB2	9 (4.6%)
IIA2	16 (8.2%)
IIB	136 (69.7%)
IIIA	8 (4.1%)
IIIB	26 (13.3%)
Median maximum tumor diameter on MRI (cm)	5 (range, 2.6–11.5)
Histotype (n)	
Squamous cell carcinoma	169 (86.7%)
Adenocarcinoma	23 (11.8%)
Others	3 (1.5%)
Tumor grade (n)	
G1	7/174 (4.0%)
G2	109/174 (62.6%)
G3	58/174 (33.3%)
pR (n)	
Complete response	86 (44.1%)
pR1 (≤3 mm)	45 (23.1%)
pR2 (>3 mm)	64 (32.8%)
Median tumor dimension (mm)	1 (range, 0–80)
Positive pelvic or aortic lymph nodes at histology (n)	24 (12.3%)
Recurrence/progression (n)	61 (31.3%)
Site of recurrence/progression (n)	
Local (vaginal/cervical)	3/59 (5.1%)
Regional (pelvic/paraaortic)	16/59 (27.1%)
Distant (upper abdominal/extraabdominal)	25/59 (42.4%)
Local and regional	3/59 (5.1%)
Local and distant	2/59 (3.4%)
Regional and distant	8/59 (13.6%)
Local, regional and distant	2/59 (3.4%)
Cancer-specific death	39 (20.0%)
Median follow-up (mo)[†]	76.0 (95% CI, 70.7–78.7)
% probability of DFS at 6 y[‡]	65.5 (95% CI, 57.9–72.1)
% probability of OS at 6 y[‡]	77.1 (95% CI, 69.9–82.9)

*Information available for 194/195 patients.
[†]Calculated with inverse Kaplan–Meier technique.
[‡]Calculated with Kaplan–Meier method.
FIGO = International Federation of Gynecology and Obstetrics; DFS = disease-free survival; OS = overall survival.

Surgery and Histopathology

Patients underwent radical hysterectomy plus pelvic with or without aortic lymphadenectomy. Histopathologic evaluation was performed by a skilled gynecologic oncologist–pathologist. Histopathology subtype (squamous cell carcinoma, adenocarcinoma, others), tumor grade, and pelvic or paraaortic lymph nodes were assessed. Pathologic response (pR) was defined as complete (absence of any residual tumor after treatment at any site level, pR0) or partial, including microscopic (persistent
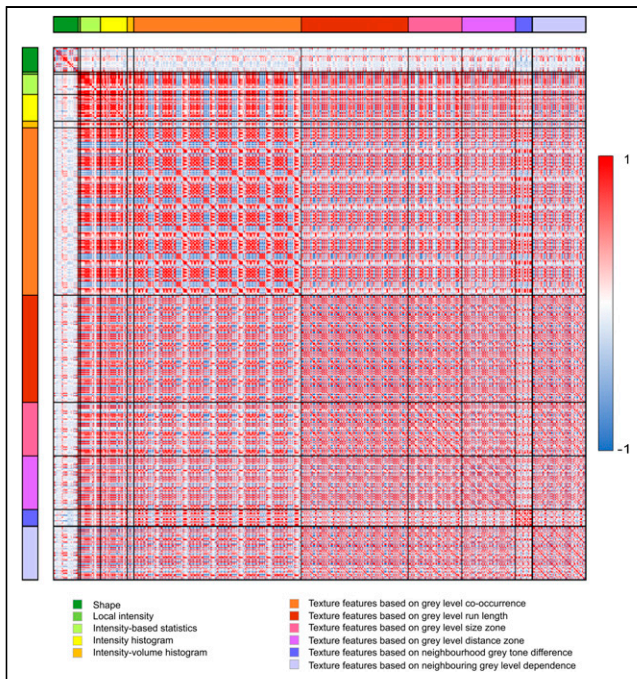
FIGURE 2. Heat map showing correlations between all radiomic features ($n = 477$). Red = high positive correlation; blue = high negative correlation; white = no correlation.

tumor foci ≤ 3 mm, pR1) and macroscopic (persistent tumor foci > 3 mm, pR2) residual tumor. pR0 and pR1 were grouped on the basis of literature results showing similar outcomes in terms of prognosis (7,33,34).

Follow-up

Patients underwent follow-up visits every 3 mo for 2 y, then every 6 mo from 2 to 5 y, and annually thereafter according to international guidelines (3). Recurrence or progression was diagnosed through biopsy or follow-up imaging. Vaginal or cervical recurrence or progression was classified as local; pelvic or paraaortic, as regional; and upper abdominal or extraabdominal, as distant (3).

Data Collection and Statistical Analysis

Data were extracted from the patients' medical records and collected using the REDCap tool hosted at https://redcap-irccs.policlinicogemelli.it (35). Study characteristics were presented as number and percentage or as median and range, as appropriate. Mean ± SD was also provided when there was a normal distribution (Shapiro–Wilk test). When necessary for readability, the original radiomic features were linearly transformed by multiplying by powers of 10. An automatic factor analysis was performed with the FMradio package for R as described by Peeters et al. (36,37), to identify the latent factors that better represented the extracted features. Detailed information about the dimensionality reduction and feature selection can be found in the supplemental materials (available at http://jnm.snmjournals.org) (36–38). The association of clinical characteristics, histopathologic parameters, and radiomic features with pathologic tumor response, disease-free survival, and overall survival was made with the Mann–Whitney U or Student t test for continuous independent variables and the Pearson χ^2 or Fisher exact test for nominal variables. Disease-free survival and overall survival were defined as the time between the date of diagnosis (biopsy) and the date of the first clinical or imaging detection of recurrence/progression and

cancer-specific death, respectively. Patients who did not experience these events were censored to the date of last follow-up or death from any cause. Median follow-up was calculated according to the inverted Kaplan–Meier technique (39). Conventional and radiomic features were dichotomized according to receiver-operating-characteristic analysis for pR and cancer-specific death prediction. Best cutoffs were chosen with Liu's method (40). Areas under the curve (AUCs) and 95% CIs were provided. An AUC of greater than 0.70 was planned for further analyses (41), including logistic and Cox regression analysis for assessing the role of dichotomized conventional and radiomic features in pR and survival prediction, respectively (42). As no AUC value reached the cutoff of 0.7, the expected analysis was no longer done. The full analysis was performed both on the whole population and separately according to the PET/CT scanner used. Statistical analyses were performed using Stata Statistical Software (release 17; StataCorp LLC). Two-sided tests were used with a significance level set at a P value of less than 0.05, and no imputation was carried out for missing data.

RESULTS

Patients and Follow-up

The records of 216 women with LACC were reviewed. Among these, 195 fulfilled the inclusion criteria (Fig. 1). Most patients had FIGO 2009 IIB stage and histologic grade 2 disease (Table 1). Squamous cell carcinoma was the most frequent histologic subtype. After surgery, 67.2% of patients had pR, including pR0 (44.1%) and pR1 (23.1%); 32.8% had pathologic nonresponse (pR2). Most patients (87.7%) had negative findings for pelvic and aortic lymph nodes. With a median follow-up of 76.0 mo, 31.3% of patients experienced recurrence or progression, and 20.0% died of the disease. Two patients died from other causes: 1 from osteosarcoma and 1 from myocardial infarction, 81 and 31 mo after the cervical cancer diagnosis, respectively.

[^{18}F]FDG PET/CT

Most [^{18}F]FDG PET/CT images (161/195 patients, 82.6%) were acquired on the Gemini GXL. Only 32 patients (16.4%) had high-uptake areas near the primary tumor and required manual correction of the VOI after semiautomatic delineation.

Data Dimensionality Reduction and Radiomic Feature Selection. Figure 2 shows the correlations for all radiomic features. Fifty-five features were retained after performing redundancy filtering. The Kaiser–Meyer–Olkin value of the final model was 0.9, well above the minimum threshold. Factor analysis performed on the 55 features determined 11 latent factors that explained 76% of the variance. These factors corresponded best to the following 11 radiomic features: volume, center of mass shift (CMS), spheric disproportion, flatness, skewness, contrast (2-dimensional [2D] merged neighborhood gray-tone difference matrix [NGTDM] feature [contrast$_{NGTDM}$]), normalized inverse difference moment (NIDM) (2D averaged gray-level cooccurrence matrix [GLCM] feature [NIDM$_{GLCM}$]), first measure of information correlation (FMIC) (3-dimensional [3D] averaged GLCM feature [FMIC$_{GLCM}$]), normalized zone distance nonuniformity (NZDNU) (3D gray-level distance zone matrix (GLDZM) feature [NZDNU$_{GLDZM}$]), coarseness (3D NGTDM feature [coarseness$_{NGTDM}$]), and low-dependence low–gray-level emphasis (LDLGLE) (3D merged neighborhood gray-level dependence matrix [NGLDM] feature [LDLGLE$_{NGLDM}$]).

Although CMS did not show the highest loading with one of the components, it showed the least correspondence to the other components and was therefore selected instead of the best-loading feature for the specific component, that is, large-zone high–gray-level

TABLE 2
Statistically Significant Conventional and Radiomic PET Features of Whole Study Population According to pR and Survival Outcomes

Feature	pR			Recurrence or progression			Cancer-specific death		
	Responders (n = 131)	Nonresponders (n = 64)	P	No (n = 134)	Yes (n = 61)	P	No (n = 156)	Yes (n = 39)	P
Conventional: SUV_{mean} (g/mL)	9.05 (2.00–32.34)	8.10 (3.23–20.11)	0.039*	8.98 (2.00–32.34)	8.64 (2.50–21.85)	0.427	9.00 (2.00–32.34)	8.01 (2.50–15.48)	0.285
Radiomic									
Shape: CMS	1.97 (0.66–14.36)	2.25 (0.93–7.09)	0.035*	1.98 (0.66–14.36)	2.36 (0.81–7.09)	0.014*	2.05 (0.66–14.36)	2.35 (0.81–7.09)	0.074
Texture									
Normalized inverse difference moment (2D averaged GLCM feature) $\times 10^2$	99.61 (94.86–99.87)	99.68 (94.39–99.88)	0.013*	99.62 (94.86–99.83)	99.67 (94.39–99.88)	0.126	99.61 (94.86–99.83)	99.68 (94.39–99.88)	0.010*
Contrast (2D merged NGTDM feature) $\times 10^2$	10.52 (2.10–103.02)	8.54 (1.82–20.38)	0.0007*	10.07 (2.13–60.57)	8.54 (1.82–103.02)	0.023*	9.99 (2.10–103.02)	8.00 (1.82–29.79)	0.010*
Normalized zone distance nonuniformity (3D GLDZM feature) $\times 10^2$	43.74 (22.97–100.00)	47.91 (20.70–100.00)	0.040*	44.50 (20.70–100.00)	45.33 (22.49–83.75)	0.434	44.39 (20.70–100.00)	47.00 (33.73–83.75)	0.119

*Statistically significant difference, calculated with 2-sided Mann–Whitney U test.
Data are median followed by range in parentheses.
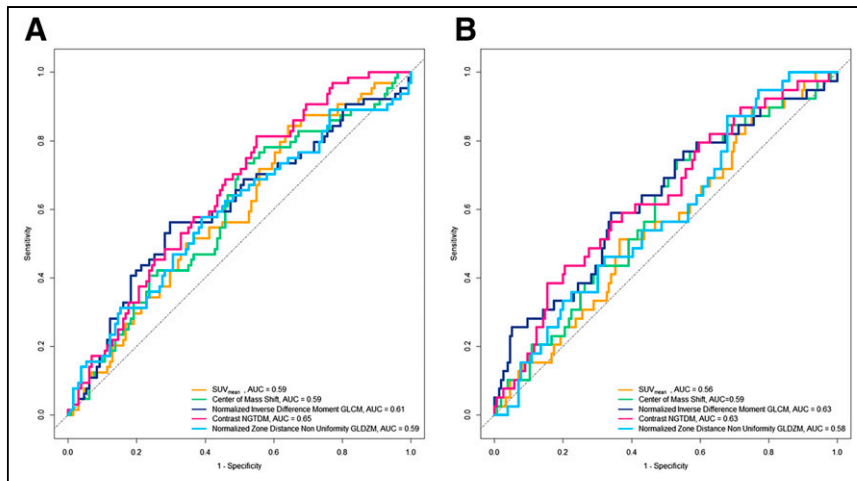
FIGURE 3. Receiver-operating-characteristics curves according to pR (A) and cancer-specific death (B).

emphasis (2D merged gray-level size zone matrix feature). A subanalysis was conducted on the Gemini GXL PET/CT cohort only (Supplemental Table 1 provides clinical data), as the sample size of the Biograph mCT cohort was too limited to perform statistical analysis separately. Ten features were selected, 5 of which had already been selected in the whole analysis ($NZDNU_{GLDZM}$, skewness, $contrast_{NGTDM}$, $coarseness_{NGTDM}$, and $FMIC_{GLCM}$) and 5 of which were different (area density axis-aligned bounding box, volume density axis-aligned bounding box, minimum intensity, large-distance low–gray-level emphasis [3D GLDZM feature], and gray-level nonuniformity [2D averaged GLDZM feature]).

Radiomic Feature Results. Among conventional features, SUV_{mean} was statistically significantly higher in patients achieving pR0–pR1 than in those with pR2 ($P = 0.039$), whereas there were no statistically significant differences in SUV_{max}, SUV_{peak}, metabolically active tumor volume, and total lesion glycolysis values between the 2 groups of each comparison (Table 2; Supplemental Table 2). In the inferential analysis of the whole cohort, among radiomic features, $contrast_{NGTDM}$ was significantly higher in responders than in nonresponders, in patients without recurrence or progression than in those with recurrence or progression, and in surviving patients than in those who had died from the disease. The opposite behavior was found for CMS, $NIDM_{GLCM}$, and $NZDNU_{GLDZM}$ (Table 2; Supplemental Table 2). Supplemental Table 3 shows the results of statistical analysis of conventional and radiomic features in the Gemini GXL PET/CT cohort, with similar findings for SUV_{mean} and the same radiomic features that were selected in both cohorts. The best cutoffs for conventional PET and radiomic features according to pR and cancer-specific death, and the relative AUCs of receiver-operating-characteristic analysis, are reported in Supplemental Tables 4 and 5 (*40*). All the AUCs were below 0.70; therefore, according to the study protocol, no further analysis was performed (Fig. 3).

DISCUSSION

This study explored the role of radiomic features extracted from pretreatment PET images to predict histo-pR and survival in LACC patients treated with neoadjuvant chemoradiotherapy followed by radical surgery. Among conventional PET parameters, SUV_{mean} was the only discriminator between responder and nonresponder

patients. Surprisingly, higher values were found in responders. Conversely, Yang et al. showed that none of the conventional PET parameters were associated with a significant difference between the 2 groups, even though in this study response assessment was imaging-based rather than histopathology-based (*14*). When applying PET-derived parameters in clinical practice, we must consider that [^{18}F]FDG uptake into tumor cells depends on many factors such as upregulation of glucose transporters and hexokinase enzymes, neoangiogenesis, and other factors, which in turn are related to tumor aggressiveness and proliferative activity (*27,43*). At the same time, many factors are responsible for intratumoral heterogeneity, such as necrosis, cellular proliferation, energy metabolism, oxygenation, and neoangiogenesis, which have been associated with tumor aggressiveness and influence biologic behavior and treatment response variability (*44,45*). Therefore, it is of clinical relevance to explore the biologic significance of functional imaging parameters and to evaluate intratumoral heterogeneity before treatment, thus allowing tailored management and improvement of outcome.

Among radiomic features, 1 shape and 3 textural features significantly differed between responders and nonresponders. The shape feature selected in our study was CMS, describing the spatial distribution of low- and high-intensity regions within the VOI; higher values are expected in nonresponders. The 3 textural features selected were $NIDM_{GLCM}$, $NZDNU_{GLDZM}$, and $contrast_{NGTDM}$. $NIDM_{GLCM}$ is a textural feature derived from GLCM matrix measuring the local homogeneity in the gray-level pattern; therefore, higher values are expected in responders. $NZDNU_{GLDZM}$ is a textural feature derived from the GLDZ matrix, measuring the distribution of groups of voxels with the same gray level and the same distance from the VOI edge. $Contrast_{NGTDM}$ is a texture feature derived from NGTD matrix describing the spatial frequency of intensity changes (*11*). Therefore, higher values are expected for these 2 latter features in nonresponders. On the basis of these explanations, the results for CMS and $NZDNU_{GLDZM}$ were no surprise, as higher values were found in nonresponders, indicating that the patterns of intratumoral [^{18}F]FDG uptake at baseline would be more heterogeneous at a regional level. Conversely, $NIDM_{GLCM}$ and $contrast_{NGTDM}$ results were not in line with expectations. In our series, 3 radiomic features significantly differed between presence and absence of recurrence or progression and between presence and absence of cancer-specific death groups. Also in this case, discrepancies were found. As expected, we observed higher CMS values in patients with a worse prognosis, whereas $NIDM_{GLCM}$ and $contrast_{NGTDM}$ values were not as expected.

We chose to dichotomize the conventional and radiomic features according to receiver-operating-characteristic analysis to retrieve cutoffs, which are a tool immediately usable by physicians for incorporating the results into clinical decision-making algorithms. Indeed, this is one of the major challenges of radiomics. The AUCs, a measure of predictive performance, were less than 0.70 for all parameters. According to the study protocol, univariate and multivariate logistic regression analyses were not performed, indicating that no conventional or radiomic features were predictive of pR and survival.

TABLE 3
Characteristics of Current and Previous Studies

Author	Study design	No. of patients	FIGO stage	Primary treatment	Imaging	Training/ validation set	Outcomes	Follow-up (mo)	Feature type	Best AUC
Yang et al. (13)	Retrospective	20	IB1-IVA	CCRT + BT	PET	No	RTT	—	6 texture features	NA
Yang et al. (14)	Retrospective	90	IB2-IVA	CCRT + BT	PET	No	RTT	—	4 texture features	RTT (energy$_{GLCM}$) = 0.659 (0.534–0.756)
Ho et al. (15)	Prospective	44	IB-IIIB	CCRT + BT	PET	No	RTT; OS	56 (10-83)	4 texture features	RTT (GLNU$_{GLRLM}$) = 0.76 (0.56-0.88)
Reuzé et al. (16)	Retrospective	118	IB1-IVB	CCRT + BT	PET	Group 1 = 79; group 2 = 39	LR	36 (median)	Mixed*	LR = 0.86 (0.75-0.97)
Altazi et al. (17)	Retrospective	80	IB-IVA	CCRT + BT	PET	TS = 56; VS = 24	DM; LRR	19 (mean)	Mixed*	DM = 0.92 (SE 0.07); LRR = 0.92 (SE 0.05)
Chen et al. (18)	Retrospective	142	IB-IIIB	CCRT + BT	PET	TS = 77; VS = 65	OS; PFS; DMFS; PRFS	40 (7-84)	7 texture features	PRFS (HGRE$_{GLRLM}$) = 0.31; PFS = 0.36
Schernberg et al. (19)	Retrospective	108	IB1-IVA	CCRT + BT	PET	TS = 69; VS = 39	LRC; OS	TS = 57.0 (6.8-100.6); VS = 30.8 (5.0-60.0)	Mixed*	NA
Lucia et al. (20)	Retrospective	102	IB1-IVA	CCRT + BT	PET; MRI	TS = 69; VS = 33	DFS; LRC	TS = 36 (6-79);VS = 17 (6-30)	1 texture feature	LRC (GLNU$_{GLRLM}$) = 0.95
Lucia et al. (21)	Retrospective multicenter	190	IB1-IVA	CCRT + BT	PET; MRI	TS = 112; VS = 78	DFS; LRC	TS = 24.3 (6.0-83.0); VS1 = 33 (14-50); VS2 = 26 (7-86)	Mixed*	LRC = 0.93
Mu et al. (22)	Retrospective multicenter	154	IIB-IVA	CCRT + BT	PET; CT	TS = 78; VS = 76	PFS; OS	TS = 28 (15-39); VS = 25 (15-36)	Mixed*	PFS = 0.72OS = 0.79
Ferreira et al. (23)	Retrospective multicenter	158	IB1-IVA	CCRT + BT	PET	TS 80%; VS 20%	DFS	23 (4-84)	Mixed*	DFS = 0.78 (0.67-0.88)
de Alencar et al. (24)	Retrospective	47	IB2-IVA	CCRT + BT	PET	No	OS	23.5 (3.7-39.0)	3 texture features	OS (LRLGE$_{GLRLM}$) = 0.74
Cho et al. (25)	Retrospective multicenter	68	IIB-IVA	CCRT + BT	PET	No	OS; PFS	49 (12-139)	1 texture feature	PFS (GLNU$_{GLRLM}$) = 0.85 (0.74-0.92)
Current study	Retrospective	195	IB2-IIIB	CRT + surgery	PET	No	pR; DFS; OS	76.0 (70.7-78.7)	1 shape and 3 texture features	pR = 0.65 (0.57-0.73); OS = 0.63 (0.54-0.73)

*Radiomic signature models with or without clinical, CT, or MRI features.

FIGO = International Federation of Gynecology and Obstetrics; CCRT = concurrent chemoradiotherapy; BT = brachytherapy; RTT = response to treatment; NA = not available; energy$_{GLCM}$ = energy derived from gray-level cooccurrence matrix; OS = overall survival; GLNU = gray-level nonuniformity; GLRLM = gray-level run-length matrix; LR = local recurrence; TS = training set; VS = validation set; DM = distant metastasis; LRR = locoregional recurrence; OS = overall survival; PFS = progression-free survival; DMFS = distant metastasis-free survival; PRFS = pelvic relapse-free survival; HGRE = high gray-level run emphasis; LRC = locoregional control; DFS = disease-free survival; LRLGE = long runs gray-level emphasis.

Several articles regarding PET radiomics in LACC patients have been published (Table 3). Just 1 study had a prospective design (*15*). Only 3 studies investigated PET radiomic features to predict response (*13–15*), whereas most assessed PET radiomic features to predict outcome (*15–25*). In most studies, texture features were significantly predictive of outcome, mainly progression-free survival and overall survival. According to Lucia et al., added value might be derived from the combination of PET and MRI radiomic features, as these 2 techniques are currently performed in standard clinical care (*20,21*). Only the study by Ferreira et al. was in line with our results, showing that no individual radiomic or clinical features were significantly associated with cancer recurrence (*23*). Importantly, the previous studies show huge variability regarding study protocol, image acquisition parameters, extraction and reduction of radiomic features, type of validation methods, and clinical outcome, affecting the reproducibility and robustness of radiomics (*8,46,47*) and emphasizing the need for further standardization of radiomic research to facilitate direct comparisons. Parallel to these considerations, we believe that our results, albeit negative, might impact current and future investigations, with the ultimate goal of exploring the biologic mechanisms underlying radiomic results (*48*).

This study had several strengths, the first being the novelty of using PET radiomic features to predict the pR in LACC patients undergoing chemoradiotherapy followed by radical surgery. A second strength was that the study included the—to our knowledge—largest cohort of LACC patients with the longest follow-up (*13–25*). Another strength was that a fixed-threshold approach was used to segment the primary tumor, which led to consistent results in the radiomic characteristics extracted from PET images (*49*). All features were extracted using software (*32*) that complies with the guidelines of the Imaging Biomarker Standardization Initiative (*11*). In radiomic studies, the problem of multiple testing or multicollinearity yields the problem of results that are falsely statistically significant (*38,49*). We addressed this problem by performing dimensionality reduction, leaving only 11 imaging features that explained most of the variance of our dataset.

This study also had some limitations. The first was its retrospective nature, like most radiomic studies (*13,14,16–25*). Second, we chose not to split our cohort into training and testing (internal validation) sets because of the limited number of events and the poor-to-moderate accuracy of the AUCs retrieved (*50*). We intend to further validate our findings in an external cohort of patients in a prospective multicenter study. Third, PET/CT images were acquired using 2 different PET/CT scanners. Nevertheless, all images were reconstructed in accordance with the European Association of Nuclear Medicine Research Ltd. standard (*28*), which has been shown to harmonize a wide range of radiomic features (*51*). Alternatively, when European Association of Nuclear Medicine Research Ltd.–compliant reconstructions are not available, radiomic features can be harmonized using ComBat (*52*).

CONCLUSION

One of the major challenges of radiomics is its incorporation into clinical decision-making algorithms for routine application. Our results in LACC patients treated by chemoradiotherapy followed by surgery indicate that this goal has not yet been reached, as [^{18}F]FDG PET radiomic features could not predict histopathologic tumor response and survival up front. In this setting, it is crucial to further explore the biologic significance of image-derived parameters and plan a large, prospective, multicenter study with standardized protocols for all phases of radiomic analysis (from image acquisition to tumor segmentation, image processing, feature extraction and reduction, and model evaluation) to assess the impact of radiomics on personalized medicine and definitively validate its use in clinical routine.

DISCLOSURE

KEY POINTS

QUESTION: Does upfront PET radiomics predict treatment response and survival in LACC?

PERTINENT FINDINGS: Our retrospective study demonstrated that no radiomic features extracted from upfront PET/CT could predict pathologic tumor response or survival in 195 patients with LACC.

IMPLICATIONS FOR PATIENT CARE: Our negative results suggest that radiomic implementation in clinical routine is still a challenge and needs to be addressed by exploring the biologic significance of image-derived parameters and by performing a prospective, multicenter study with standardized protocols for all phases of radiomic analysis.

REFERENCES

1. Sung H, Ferlay J, Siegel RL, et al. Global cancer statistics 2020: GLOBOCAN estimates of incidence and mortality worldwide for 36 cancers in 185 countries. *CA Cancer J Clin.* 2021;71:209–249.
2. Cibula D, Raspollini MR, Planchamp F, et al. ESGO/ESTRO/ESP guidelines for the management of patients with cervical cancer: update 2023. *Int J Gynecol Cancer.* 2023;33:649–666.
3. Abu-Rustum NR, Yashar CM, Arend R, et al. NCCN clinical practice guidelines in oncology (NCCN guidelines): cervical cancer—version 2.2024. National Comprehensive Cancer Network website. https://www.nccn.org/professionals/physician_gls/pdf/cervical.pdf. Published February 23, 2024. Accessed March 19, 2024.
4. Grigsby PW. The prognostic value of PET and PET/CT in cervical cancer. *Cancer Imaging.* 2008;8:146–155.
5. Espenel S, Garcia MA, Trone JC, et al. From IB2 to IIIB locally advanced cervical cancers: report of a ten-year experience. *Radiat Oncol.* 2018;13:16.
6. Ferrandina G, Legge F, Fagotti A, et al. Preoperative concomitant chemoradiotherapy in locally advanced cervical cancer: safety, outcome, and prognostic measures. *Gynecol Oncol.* 2007;107(suppl 1):S127–S132.
7. Federico A, Anchora LP, Gallotta V, et al. Clinical impact of pathologic residual tumor in locally advanced cervical cancer patients managed by chemoradiotherapy followed by radical surgery: a large, multicenter, retrospective study. *Ann Surg Oncol.* 2022;29:4806–4814.
8. Lambin P, Leijenaar RTH, Deist TM, et al. Radiomics: the bridge between medical imaging and personalized medicine. *Nat Rev Clin Oncol.* 2017;14:749–762.
9. Hatt M, Le Rest CC, Tixier F, Badic B, Schick U, Visvikis D. Radiomics: data are also images. *J Nucl Med.* 2019;60(suppl 2):38S–44S.
10. Mayerhoefer ME, Materka A, Langs G, et al. Introduction to radiomics. *J Nucl Med.* 2020;61:488–495.
11. Zwanenburg A, Vallières M, Abdalah MA, et al. The image biomarker standardization initiative: standardized quantitative radiomics for high-throughput image-based phenotyping. *Radiology.* 2020;295:328–338.
12. Hatt M, Tixier F, Pierce L, Kinahan PE, Le Rest CC, Visvikis D. Characterization of PET/CT images using texture analysis: the past, the present … any future? *Eur J Nucl Med Mol Imaging.* 2017;44:151–165.
13. Yang F, Thomas MA, Dehdashti F, Grigsby PW. Temporal analysis of intratumoral metabolic heterogeneity characterized by textural features in cervical cancer. *Eur J Nucl Med Mol Imaging.* 2013;40:716–727.

14. Yang F, Young L, Grigsby P. Predictive value of standardized intratumoral metabolic heterogeneity in locally advanced cervical cancer treated with chemoradiation. *Int J Gynecol Cancer.* 2016;26:777–784.

15. Ho K-C, Fang Y-HD, Chung H-W, et al. A preliminary investigation into textural features of intratumoral metabolic heterogeneity in ^{18}F-FDG PET for overall survival prognosis in patients with bulky cervical cancer treated with definitive concurrent chemoradiotherapy. *Am J Nucl Med Mol Imaging.* 2016;6:166–175.

16. Reuzé S, Orlhac F, Chargari C, et al. Prediction of cervical cancer recurrence using textural features extracted from ^{18}F-FDG PET images acquired with different scanners. *Oncotarget.* 2017;8:43169–43179.

17. Altazi BA, Fernandez DC, Zhang GG, et al. Investigating multi-radiomic models for enhancing prediction power of cervical cancer treatment outcomes. *Phys Med.* 2018;46:180–188.

18. Chen S-W, Shen W-C, Hsieh T-C, et al. Textural features of cervical cancers on FDG-PET/CT associate with survival and local relapse in patients treated with definitive chemoradiotherapy. *Sci Rep.* 2018;8:11859.

19. Schernberg A, Reuze S, Orlhac F, et al. A score combining baseline neutrophilia and primary tumor SUVpeak measured from FDG PET is associated with outcome in locally advanced cervical cancer. *Eur J Nucl Med Mol Imaging.* 2018;45:187–195.

20. Lucia F, Visvikis D, Desseroit MC, et al. Prediction of outcome using pretreatment ^{18}F-FDG PET/CT and MRI radiomics in locally advanced cervical cancer treated with chemoradiotherapy. *Eur J Nucl Med Mol Imaging.* 2018;45:768–786.

21. Lucia F, Visvikis D, Vallières M, et al. External validation of a combined PET and MRI radiomics model for prediction of recurrence in cervical cancer patients treated with chemoradiotherapy. *Eur J Nucl Med Mol Imaging.* 2019;46:864–877.

22. Mu W, Liang Y, Hall LO, et al. ^{18}F-FDG PET/CT habitat radiomics predicts outcome of patients with cervical cancer treated with chemoradiotherapy. *Radiol Artif Intell.* 2020;2:e190218.

23. Ferreira M, Lovinfosse P, Hermesse J, et al. [^{18}F]FDG PET radiomics to predict disease-free survival in cervical cancer: a multi-scanner/center study with external validation. *Eur J Nucl Med Mol Imaging.* 2021;48:3432–3443.

24. de Alencar NRG, Machado MAD, Mourato FA, et al. Exploratory analysis of radiomic as prognostic biomarkers in ^{18}F-FDG PET/CT scan in uterine cervical cancer. *Front Med (Lausanne).* 2022;9:1046551.

25. Cho H-W, Lee ES, Lee JK, Eo JS, Kim S, Hong JH. Prognostic value of textural features obtained from F-fluorodeoxyglucose (F-18 FDG) positron emission tomography/computed tomography (PET/CT) in patients with locally advanced cervical cancer undergoing concurrent chemoradiotherapy. *Ann Nucl Med.* 2023; 37:44–51.

26. Hatt M, Majdoub M, Vallières M, et al. ^{18}F-FDG PET uptake characterization through texture analysis: investigating the complementary nature of heterogeneity and functional tumor volume in a multi-cancer site patient cohort. *J Nucl Med.* 2015;56:38–44.

27. Rufini V, Collarino A, Calcagni ML, et al. The role of ^{18}F-FDG-PET/CT in predicting the histopathological response in locally advanced cervical carcinoma treated by chemo-radiotherapy followed by radical surgery: a prospective study. *Eur J Nucl Med Mol Imaging.* 2020;47:1228–1238.

28. Boellaard R, Delgado-Bolton R, Oyen WJG, et al. FDG PET/CT: EANM procedure guidelines for tumour imaging—version 2.0. *Eur J Nucl Med Mol Imaging.* 2015;42:328–354.

29. Boellaard R. Quantitative oncology molecular analysis suite: ACCURATE [abstract]. *J Nucl Med.* 2018;59(suppl 1):1753.

30. Collarino A, Garganese G, Fragomeni SM, et al. Radiomics in vulvar cancer: first clinical experience using ^{18}F-FDG PET/CT images. *J Nucl Med.* 2018;60:199–206.

31. Frings V, Van Velden FHP, Velasquez LM, et al. Repeatability of metabolically active tumor volume measurements with FDG PET/CT in advanced gastrointestinal malignancies: a multicenter study. *Radiology.* 2014;273:539–548.

32. Pfaehler E, Zwanenburg A, de Jong JR, Boellaard R. RACAT: an open source and easy to use radiomics calculator tool. *PLoS One.* 2019;14:e0212223.

33. Ferrandina G, Margariti PA, Smaniotto D, et al. Long-term analysis of clinical outcome and complications in locally advanced cervical cancer patients administered concomitant chemoradiation followed by radical surgery. *Gynecol Oncol.* 2010; 119:404–410.

34. Zannoni GF, Vellone VG, Carbone A. Morphological effects of radiochemotherapy on cervical carcinoma: a morphological study of 50 cases of hysterectomy specimens after neoadjuvant treatment. *Int J Gynecol Pathol.* 2008;27:274–281.

35. Harris PA, Taylor R, Thielke R, Payne J, Gonzalez N, Conde JG. Research electronic data capture (REDCap): a metadata-driven methodology and workflow process for providing translational research informatics support. *J Biomed Inform.* 2009;42:377–381.

36. Peeters CFW, Übelhör C, Mes SW, et al. Stable prediction with radiomics data. arXiv website. https://doi.org/10.48550/arXiv.1903.11696. Published March 27, 2019. Accessed March 19, 2024.

37. The R project for statistical computing. R Foundation website. https://www.R-project.org/. Accessed March 19, 2024.

38. Chalkidou A, O'Doherty MJ, Marsden PK. False discovery rates in PET and CT studies with texture features: a systematic review. *PLoS One.* 2015;10:e0124165.

39. Schemper M, Smith TL. A note on quantifying follow-up in studies of failure time. *Control Clin Trials.* 1996;17:343–346.

40. Liu X. Classification accuracy and cut point selection. *Stat Med.* 2012;31:2676–2686.

41. Hosmer DW, Lemeshow S. Assessing the fit of the model. In: *Applied Logistic Regression.* John Wiley & Sons, Ltd; 2000:160–164.

42. Cox DR. Regression models and life-tables. *J R Stat Soc Series B Stat Methodol.* 1972;34:187–202.

43. Bos R, van Der Hoeven JJM, van Der Wall E, et al. Biologic correlates of [18]fluorodeoxyglucose uptake in human breast cancer measured by positron emission tomography. *J Clin Oncol.* 2002;20:379–387.

44. Pugachev A, Ruan S, Carlin S, et al. Dependence of FDG uptake on tumor microenvironment. *Int J Radiat Oncol Biol Phys.* 2005;62:545–553.

45. Zhao S, Kuge Y, Mochizuki T, et al. Biologic correlates of intratumoral heterogeneity in ^{18}F-FDG distribution with regional expression of glucose transporters and hexokinase-II in experimental tumor. *J Nucl Med.* 2005;46:675–682.

46. Vallières M, Zwanenburg A, Badic B, Cheze Le Rest C, Visvikis D, Hatt M. Responsible radiomics research for faster clinical translation. *J Nucl Med.* 2018;59: 189–193.

47. Sollini M, Antunovic L, Chiti A, Kirienko M. Towards clinical application of image mining: a systematic review on artificial intelligence and radiomics. *Eur J Nucl Med Mol Imaging.* 2019;46:2656–2672.

48. Buvat I, Orlhac F. The dark side of radiomics: on the paramount importance of publishing negative results. *J Nucl Med.* 2019;60:1543–1544.

49. Limkin EJ, Sun R, Dercle L, et al. Promises and challenges for the implementation of computational medical imaging (radiomics) in oncology. *Ann Oncol.* 2017;28: 1191–1206.

50. Swets JA. Indices of discrimination or diagnostic accuracy: their ROCs and implied models. *Psychol Bull.* 1986;99:100–117.

51. Pfaehler E, van Sluis J, Merema BBJ, et al. Experimental multicenter and multivendor evaluation of the performance of PET radiomic features using 3-dimensionally printed phantom inserts. *J Nucl Med.* 2020;61:469–476.

52. Orlhac F, Eertink JJ, Cottereau AS, et al. A guide to ComBat harmonization of imaging biomarkers in multicenter studies. *J Nucl Med.* 2022;63:172–179.